Alqalam Journal of Medical and Applied Sciences. 2026;9(11):3904-3915
https://doi.org/10.54361/ajmas.261148

Original article

Effects of Zinc Doping on The Superconducting Properties of $YBa_2(Cu_{1-X}Zn_x)_3O_{7-\delta}$ (X= 0, 0.01, 0.02, 0.03)

Layla Zayed[1]*, Mabrouka Barggig[2]

[1]*Physics Department, Faculty of Education, Nalut University, Nalut, Libya*
[2]*Faculty of Science and Technology, Kebangsaan University, Bangi, Malaysia*
Email: *L.zayed@nu.edu.ly*

Abstract
This study aimed to investigate the effects of the addition of Zn in the $YBa_2(Cu_{1-x}Zn_x)_3O_{7-\delta}$ high-temperature superconductor with compositions x = 0.00, 0.01, 0.02, and 0.03. Samples with different compositions were prepared through the solid-state reaction method. The critical temperatures (T_c) of the samples were determined by the four-point probe method. The Van Der Pauw method was used to determine the resistivity of the samples at room temperature. X-ray diffraction (XRD) was used to determine the structure and phase of the samples, and scanning electron microscopy (SEM) was used to determine the morphology and microstructure of the samples. The Tc decreases from 95K to 53K with increased composition of Zn doped. Decreasing of T_c is related to two possible mechanisms; in part is due to the Zn ion acting as a strong in-plane scattering centre and, in part is due to the loss in oxygen content as Zn is substituted for Cu. These conditions may affect the magnetic pair breaking of the materials. The electrical resistivity increased from $2.2x10^{-5}$ Ω. m to $4x10^{-5}$ Ω. m with increased Zn compositions. The XRD diffraction analysis showed that all samples were single-phase with an orthorhombic structure as the Zn compositions increased. The SEM results showed a clear change in grain size between the YBCO sample and YBCO samples doped with Zn. The grain size decreased from x = 0 to x = 0.01. The change in the microstructure was due to the increase in the Zn concentration and was direct evidence of changes in the nature of the grain boundaries due to impurities.
Keywords. Zinc Doping, Superconducting Properties, High-Temperature, Grain Size.

Introduction

Superconductivity is the ability of some metals and alloys to allow electrical current flow without any electrical resistance. Superconductivity appears below a certain (critical) temperature, which is between 30K and 120K (-243°C and -153°C) for high-temperature superconductors (HTS) and below 20K (-253°C) for the low-temperature superconductors (LTS). The conduction mechanism in superconductors is entirely different from non-superconductors because in superconductors the charge carriers form pairs called Cooper pairs [1]. There are two important properties of superconductors:

The zero-dc resistivity ($\rho = 0$)

This means that an electrical current in a superconducting loop continues indefinitely until a force is applied to oppose the current. Zero resistivity occurs in superconductors because, at low temperature, the Cooper pairs are able to move without any resistance. These Cooper pairs are formed through the electron-phonon interaction. (Figure1) shows the electrical resistance versus temperature [1].

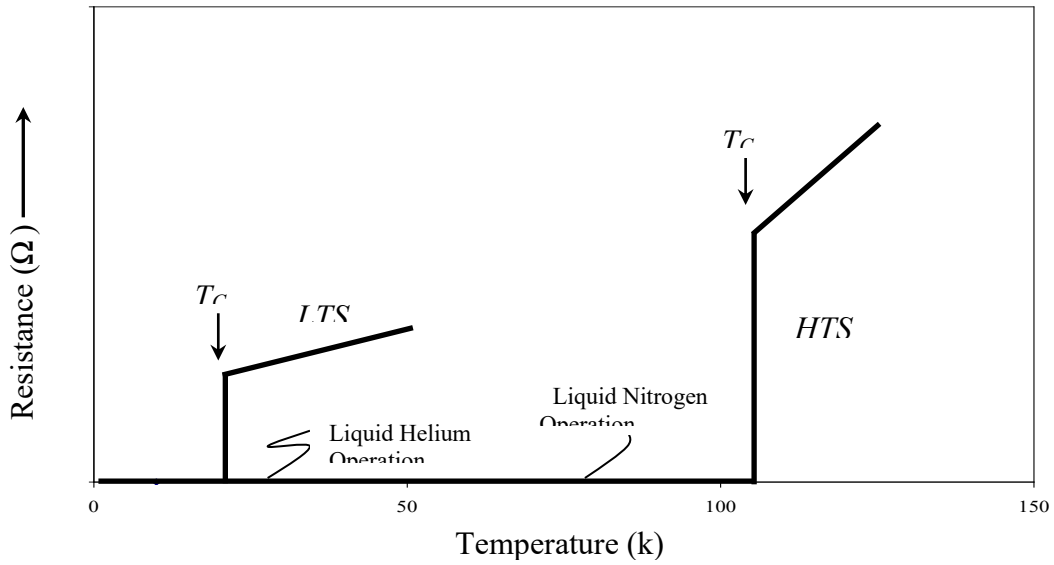

Figure 1. The differences in behavior between LTS and HTS materials

Copyright *Author (s) 2026. Distributed under Creative Commons CC BY 4.0*
Received*: 18-09-2026 -* ***Accepted****: 16-11-2026 -* ***Published****: 24-11-2026*

https://doi.org/10.54361/ajmas.261148

Perfect Diamagnetism

Perfect diamagnetism is a phenomenon occurring in some materials at low temperatures, characterised by the complete absence of magnetic permeability ($\mu = 0$) and the expulsion of the externally applied magnetic field (the Meissner effect). It was known in 1933 by Walter Meissner and Robert Ochsenfeld. Perfect diamagnetism occurs when a moderate magnetic field is applied to superconductors [2]. (Figure 2) shows the magnetic flux exclusion in a superconductor.

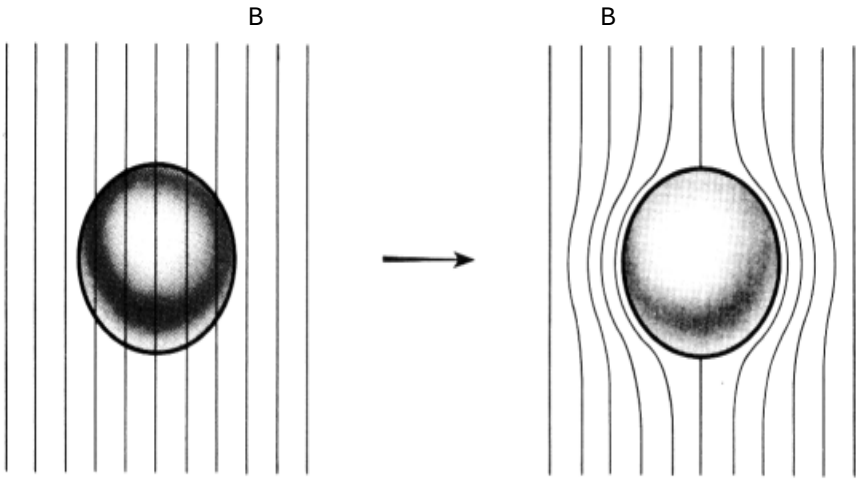

Figure2 : the magnetic flux exclusion in a superconductor

Technological applications of superconductivity

Several technological applications of superconductivity include high-speed trains, sensitive magnetometers based on SQUIDs, digital circuits, Magnetic Resonance Imaging (MRI) for medical applications, electric power transmission cables, and microwave filters (e.g., for mobile phone base stations). Commercial applications include transformers, power storage, propulsion systems for vehicles such as ships and spacecraft, electric motors, super fast computer circuits.

High-temperature oxide superconductors

High-temperature superconductors (abbreviated HTS) are materials that have a superconducting transition temperature (T_c) above 30 K, higher than the boiling point of liquid nitrogen (~ 77 K). The high-Tc superconductor was discovered in 1986 by K. Müller and J. Bednorz, for which they were awarded the Nobel Prize in Physics in 1987. The high-temperature superconductors known as Perovskites and these superconductors are a mixture of metal oxides which appear the physical properties of ceramics. The first high-temperature superconductor, La-Ba-Cu-O, with a transition temperature of 30 K, LSCO ($La_{2-x}Sr_xCuO_4$) was discovered in the same year, in 1987 – YBCO (123) was discovered to have a T_c of 90 K. In 1988, the BSCCO (2223) phase was discovered with T_c up to 108 K; the TBCCO (2223) phase was discovered to have T_c of 127 K; the HBCCO (1223) phase T_c=134K [3]. This class of materials not only show high-temperature superconductivity but also shows properties that are different from classical superconductors. This offers a great challenge to understanding the basic phenomenon that causes superconductivity in these materials and to developing the appropriate preparation methods so that these can be exploited for a wide range of applications. During the last one and a half decades after the discovery of high- T_c materials, several high- T_c superconductors have been discovered which show superconductivity at temperatures higher than liquid-nitrogen temperature (77 K); liquid nitrogen is a relatively inexpensive and easily handled coolant [4].

YBCO Superconductor

Yttrium barium copper oxide, abbreviated YBCO, is a crystalline chemical compound with several phases, such as $YBa_2Cu_3O_7$ (Y123), $Y_2Ba_4Cu_7O_{14-\delta}$ (Y247) and $YBa_2Cu_4O_{8-\delta}$ (Y124) materials were initially found by M.K.Wu et al [5]. in 1987. This material, a “high-temperature superconductor", achieved prominence because it was the first material to achieve superconductivity above the boiling point of nitrogen. Many factors affect the superconducting properties of YBCO, such as oxygen content, preparation methods involving heat treatment, composition and element substitutions [6].

Copyright *Author (s) 2026. Distributed under Creative Commons CC BY 4.0*
Received*: 18-09-2026 -* ***Accepted****: 16-11-2026 -* ***Published****: 24-11-2026*

https://doi.org/10.54361/ajmas.261148

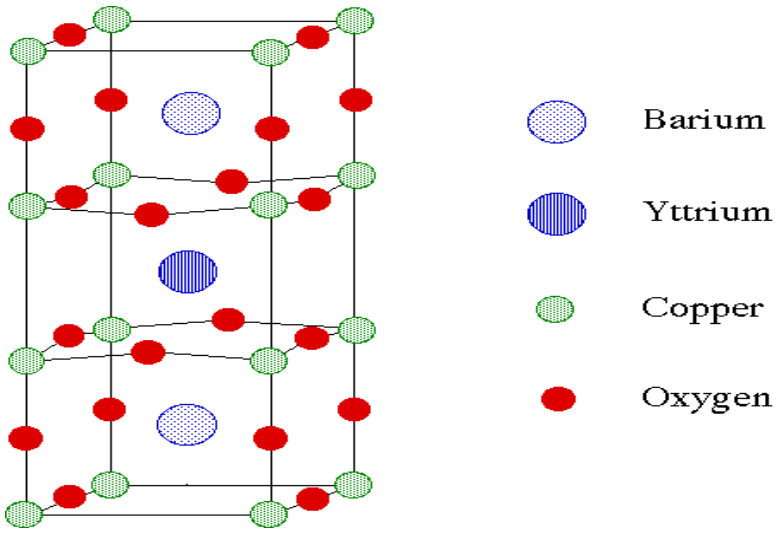

Figure3. The unit cell structure of $YBa_2Cu_3O_{7-\delta}$ [7]

The unit cell of YBCO (123) consists of three pseudocubic elementary perovskite unit cells. Each perovskite unit cell contains: Ba in the bottom unit cell, Y in the middle one, and Ba in the top unit cell. Thus, Y and Ba are stacked in the series [Ba-Y-Ba] along the c-axis [8]. The perovskite-type feature and the presence of CuO2 layers also exist in these superconductors. The dimensions of a single unit cell of YBCO are a = 3.82 Å, b = 3.89 Å, and c = 11.68 Å. The chemical formula of term 7-δ implies a slight deficiency of oxygen. If δ=0, the lattice parameters are in the orthorhombic phase, whereas in the case of δ=1, the material has a tetragonal structure. Only the orthorhombic configuration is superconducting.

Objectives of the Research

This research aims to prepare and characterise the composite $YBa_2(Cu_{1-x}Zn_x)_3O_{7-\delta}$ with x = 0.0, 0.01, 0.02, and 0.03. The study seeks to elucidate the electrical, microstructural, and structural properties, as well as the mechanisms responsible for the variation in critical temperature (T_c) in Zn-doped YBCO.

Methodology

Preparation of the Samples

The chemical equation for sample preparation is given as:

$$\frac{1}{2}Y_2O_3 + 2BaO + 3(1\text{-}x)\,CuO + 3(x)ZnO \longrightarrow YBa_2(Cu_{1-x}Zn_x)_3O_{7-\delta}.$$

$YBa_2(Cu_{1-x}Zn_x)_3O_{7-\delta}$ with (x = 0, 0.01, 0.02 and 0.03) samples were prepared by mixing appropriate amounts of high-purity (99.99%) Y_2O_3, BaO, CuO and ZnO powders. The mixed powders were heated at 900 ˚C for 48 h with several intermittent grindings and oven-cooled. The powders were pressed into pellets and heated at 900 °C in air for another 24 hours, followed by furnace cooling to room temperature.

Characterizations

The four-point probe method was employed to determine the critical temperature (T_c) of the superconductors. The resistivity (ρ of each sample was calculated using the Van der Pauw method according to the equation $\rho = (\frac{\pi\, d}{\ln 2}) \times \frac{V}{I}$, where ρ is the volume resistivity, V is the measured voltage, I is the source current, and d is the sample thickness. X-ray powder diffraction (XRD) was used as a fast analytical technique for phase identification of the crystalline material and to provide information on unit cell dimensions, with the lattice parameters a, b, and c determined from the equation:

$$\frac{1}{d_{hkl}^2} = \frac{h^2}{a^2} + \frac{k^2}{b^2} + \frac{l^2}{c^2}.$$

The scanning electron microscope (SEM), which uses electrons instead of light to form an image, was utilized to study the correlation between microstructural features—such as sample's homogeneity, grain size, and alignment related to the superconducting behaviour of the samples. The fractured surface of the sample was coated with evaporated gold prior to insertion into the microscope.

Results and Discussion

Results of critical temperature (T_c) measurements

By using the four-point probe method then obtains the critical temperature of the samples that had been prepared was obtained. A graph of resistance versus temperature was obtained. The data obtained in each graph of electrical resistance against temperature are shown in Figure 4.1 to Figure 4.4. Table2 shows the summarised data of T_c onset and zero for all

Copyright *Author (s) 2026. Distributed under Creative Commons CC BY 4.0*
Received: *18-09-2026 -* ***Accepted:*** *16-11-2026 -* ***Published:*** *24-11-2026*

https://doi.org/10.54361/ajmas.261148

samples. The normalised resistance versus temperature curve (R-T) of $YBa_2(Cu_{1-x}Zn_x)_3O_{7-}\delta$ for x = 0, 0.01, 0.02 and 0.03 is shown in (Figure 4.5). (Figure 4.6) shows a graph of $T_{c\,(onset)}$ and $T_{c\,(zero)}$ versus the composition x = 0, 0.01, 0.02 and 0.03 for the $YBa_2(Cu_{1-x}Zn_x)_3O_{7-}\delta$

Table2. $T_{c\,(onset)}$, $T_{c\,(zero)}$ and (ΔTc) for $YBa_2(Cu_{1-x}Zn_x)_3O_{7-}\delta$

Sample $YBa_2(Cu_{1-x}Zn_x)_3O_7$	T_c onset(±1K)	T_c zero(±1K)	ΔT_c(±1K)	Normal state
0.00	95	88	7	metallic
0.01	69	44	25	semimetal
0.02	58	28	29	semiconductor
0.03	53	26	27	semiconductor

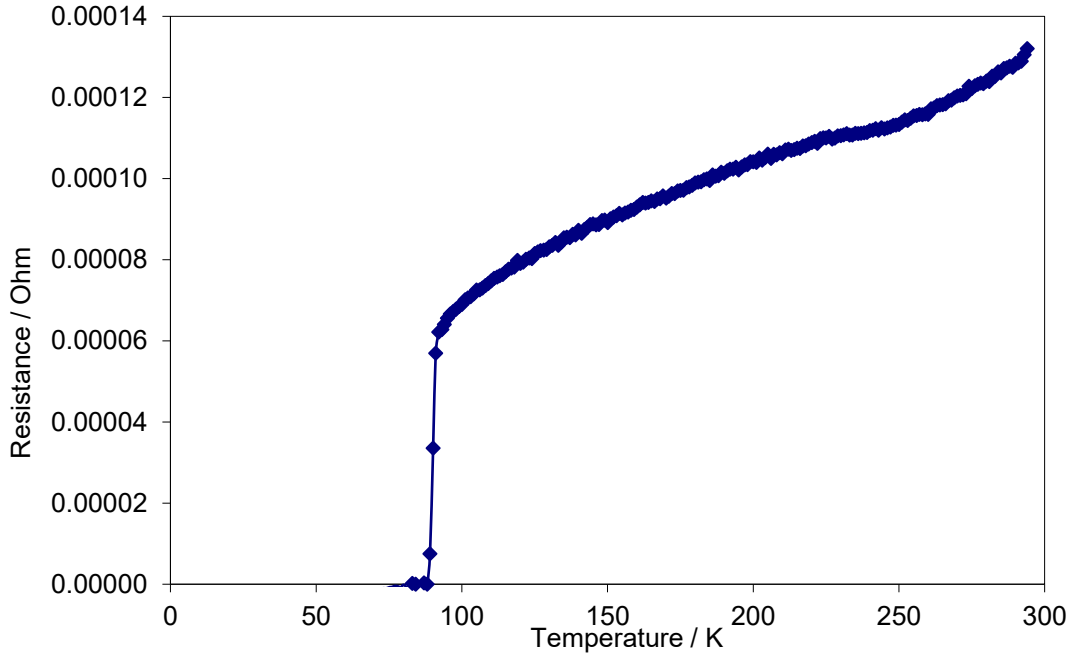

Figure 4.1. electric resistances versus temperature for $YBa_2(Cu_{1-x}Zn_x)_3O_{7-}\delta$ with composition x =0

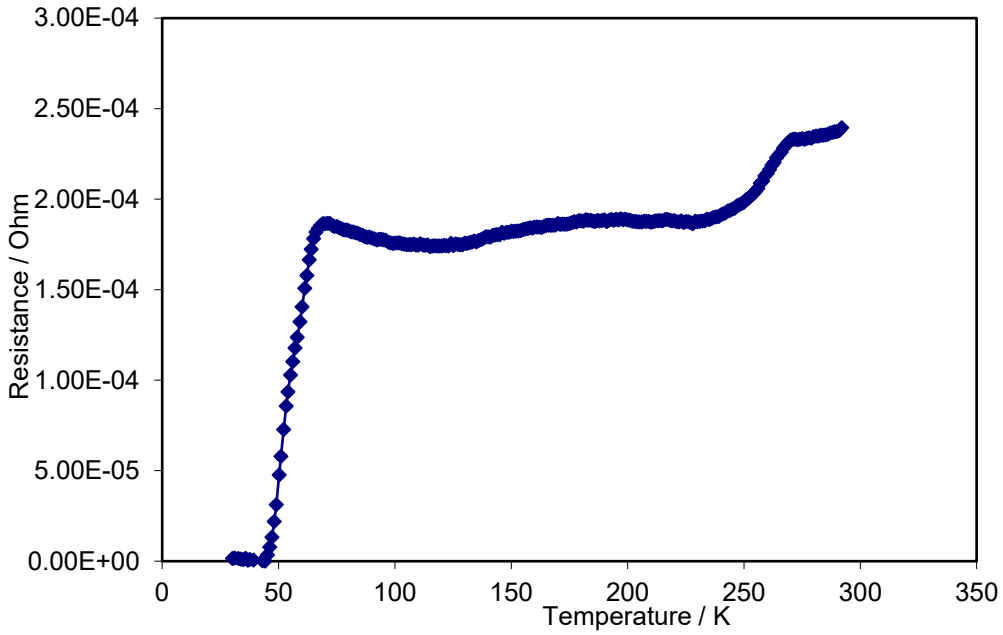

Figure 4.2. electric resistances versus temperature for $YBa_2(Cu_{1-x}Zn_x)_3O_{7-}\delta$with composition x =0.01

Copyright *Author (s) 2026. Distributed under Creative Commons CC BY 4.0*
Received: *18-09-2026 -* ***Accepted:*** *16-11-2026 -* ***Published:*** *24-11-2026*

https://doi.org/10.54361/ajmas.261148

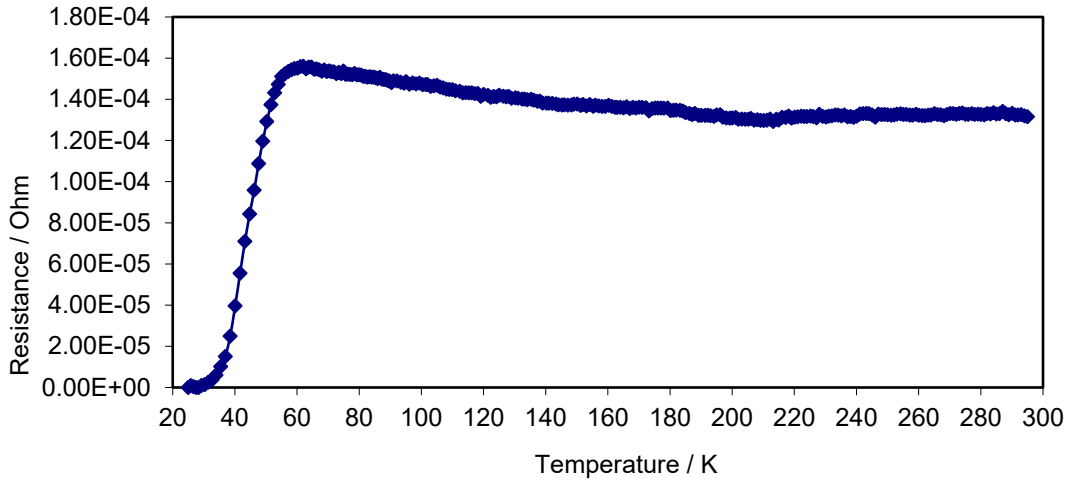

Figure 4.3. electric resistances versus temperature for $YBa_2(Cu_{1-x}Zn_x)_3O_{7-}\delta$ with composition x =0.02.

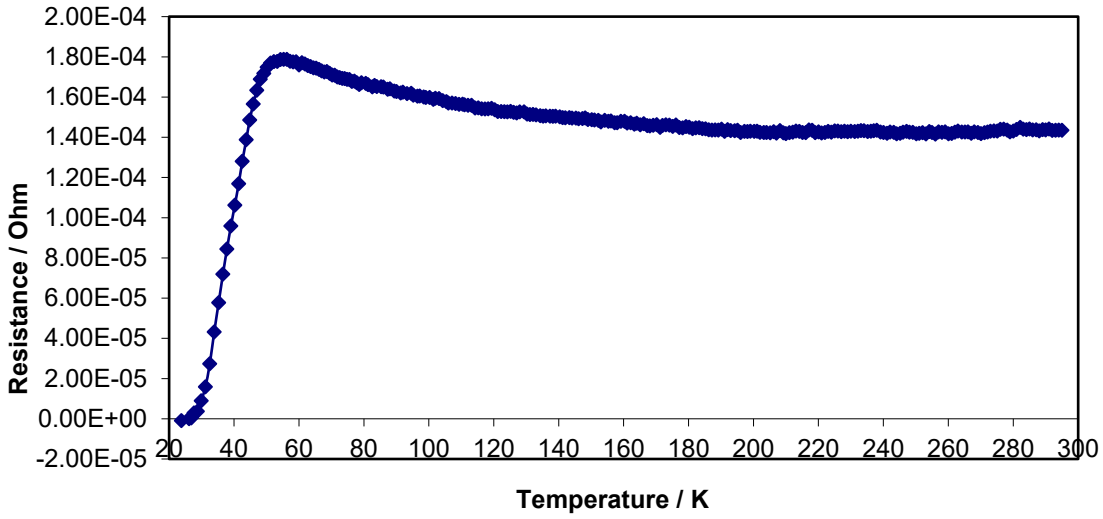

Figure 4.4. electric resistances versus temperature of $YBa_2(Cu_{1-x}Zn_x)_3O_{7-}\delta$ with composition x =0.03

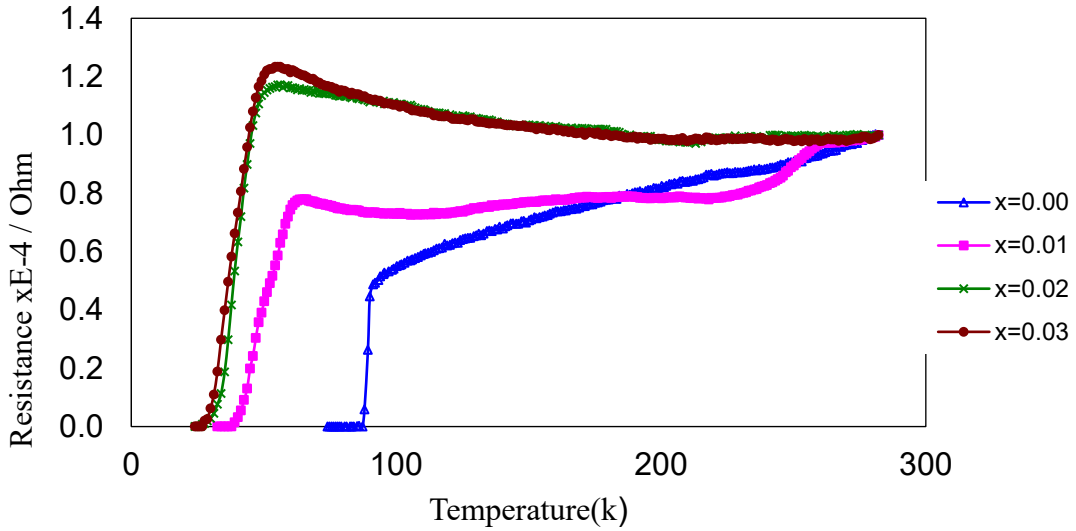

Figure 4.5. Normalised electric resistance versus temperature of $YBa_2(Cu_{1-x}Zn_x)_3O_{7-}\delta$ for (x= 0, 0.01, 0.02, 0.03)

Copyright *Author (s) 2026. Distributed under Creative Commons CC BY 4.0*
Received: *18-09-2026 -* ***Accepted:*** *16-11-2026 -* ***Published:*** *24-11-2026*

https://doi.org/10.54361/ajmas.261148

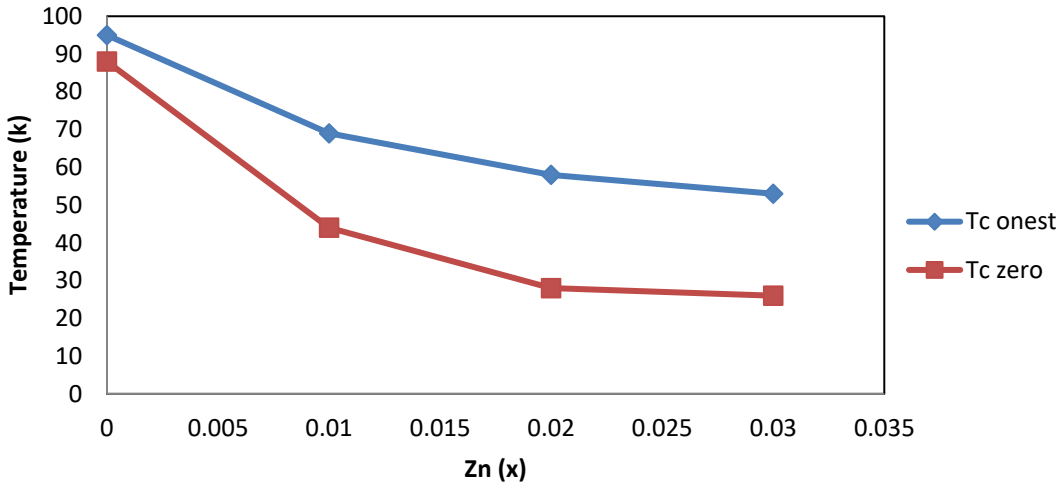

Figure 4.6. T_c (onset) and T_c (zero) versus composition (x)

The samples were heated at 900 C° for 24 hours in air. The temperature-dependent electrical resistance of $YBa_2(Cu_{1-x}Zn_x)_3O_{7-\delta}$ with x = 0, 0.01, 0.02 and 0.03 shows a change from metallic to a semiconducting behaviour with increasing Zn concentration. When the concentration is low, the normal state is metallic {(∂R/∂T)>0, and when the concentration is large, semiconducting behaviour takes place {(∂R/∂T)<0}[9]. This can be explained as a disorder due to the random distribution of inhomogeneities inside YBCO. The superconducting transition temperature, T_c onset (onset critical temperature) are 95 K, 69 K, 58 K and 53 K for x=0, 0.01, 0.02 and 0.03 respectively, and T_c zero (zero critical temperature) are 88 K, 44 K, 28 K and 24 K for x=0, 0.01, 0.02 and 0.03 respectively (Fig. 4.6). The transition width ΔT_c increases with increasing zinc content. T_c decreases rapidly with increasing zinc doping. Previous studies [10],[11] showed that the suppression of T_c can be attributed to two possible mechanisms: in part it is due to the Zn ion acting as a strong in-plane scattering centre and, in part is due to the loss in oxygen content as Zn is substituted for Cu.

Electrical Resistivity at Room Temperature

The van der Pauw method has been used to calculate the electrical resistivity at room temperature of samples $YBa_2(Cu_{1-x}Zn_x)_3O_{7-\delta}$ with composition x= 0, 0.01, 0.02, and 0.03. Table3 and Figure 5 show the results of the resistivity measurements.

Table3. Electric resistivity (ρ) with different compositions of x

Composition x	**Resistivity, $\rho \times 10^{-5}$(Ω.m)**
0	(2.2 ± 0.3)
0.01	(3.0 ± 0.3)
0.02	(3.7 ± 0.4)
0.03	(4.0 ± 0.4)

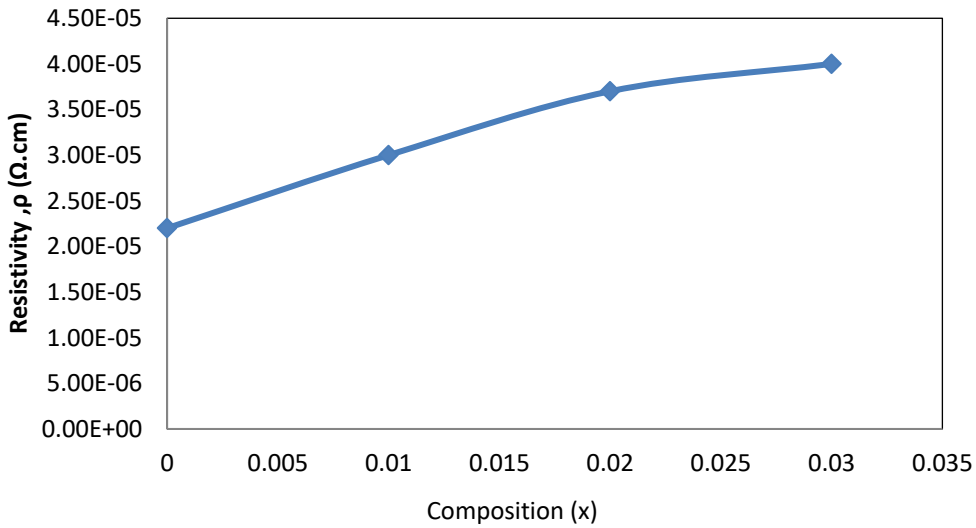

Figure5. Electrical resistivity ρ versus composition of x

Copyright *Author (s) 2026. Distributed under Creative Commons CC BY 4.0*
Received: *18-09-2026 -* ***Accepted:*** *16-11-2026 -* ***Published:*** *24-11-2026*

https://doi.org/10.54361/ajmas.261148

The results showed that the electrical resistivity of the samples at room temperature increases when Zn replaces Cu. The sample x= 0 showed the lowest resistivity value compared to other samples. The electrical resistivity of $YBa_2(Cu_{1-x}Zn_x)_3O_7-\delta$ samples with x = 0 , 0.01, 0.02 are 2.2×10^{-5} Ωm, 3×10^{-5} Ωm, 3.7×10^{-5} Ωm respectively . The sample x = 0.03 showed the highest electric resistivity 4×10^{-5} Ωm. This increase of the resistivity value with increasing x implies that the primary effect of Zn scattering is to add a nominally temperature-independent contribution to the transport scattering rate [12].

X-ray diffraction (XRD)

(Figure 6.1) shows X-ray diffraction patterns for pure and Zn substitution samples.

Table4. lattice parameter a, b and c for $YBa_2(Cu_{1-x}Zn_x)_3O_7-\delta$ with different composition

Sample $YBa_2Cu_3O_7$	a(A°)	b (A°)	c(A°)	Ratio c/b	volume A^3
0	3.824±0.001	3.878±0.002	11.678±0.003	3	173.2
0.01	3.831±0.003	3.873±0.006	11.691±0.004	3	173.5
0.02	3.831±0.003	3.873±0.004	11.673±0.004	3	173.2
0.03	3.834±0.005	3.876±0.004	11.672±0.004	3	173.5

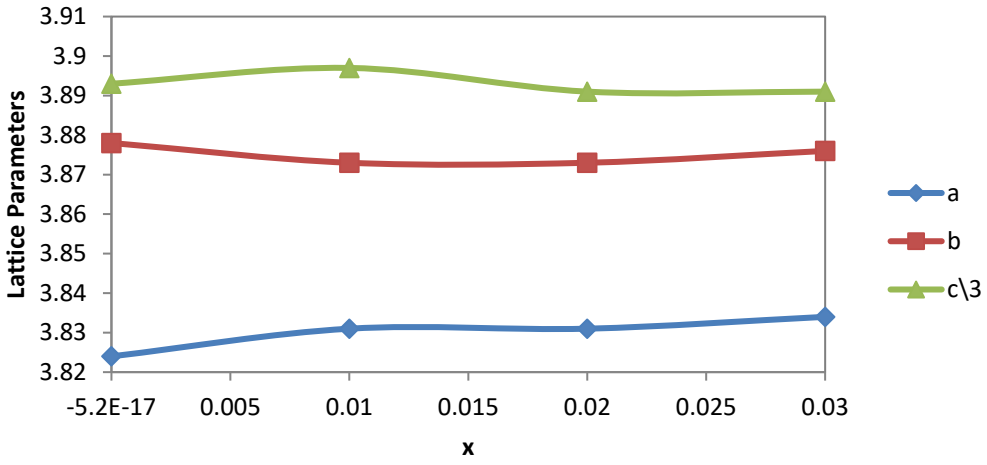

Figure6.1. lattice parameter a, b and c/3 versus composition (x)

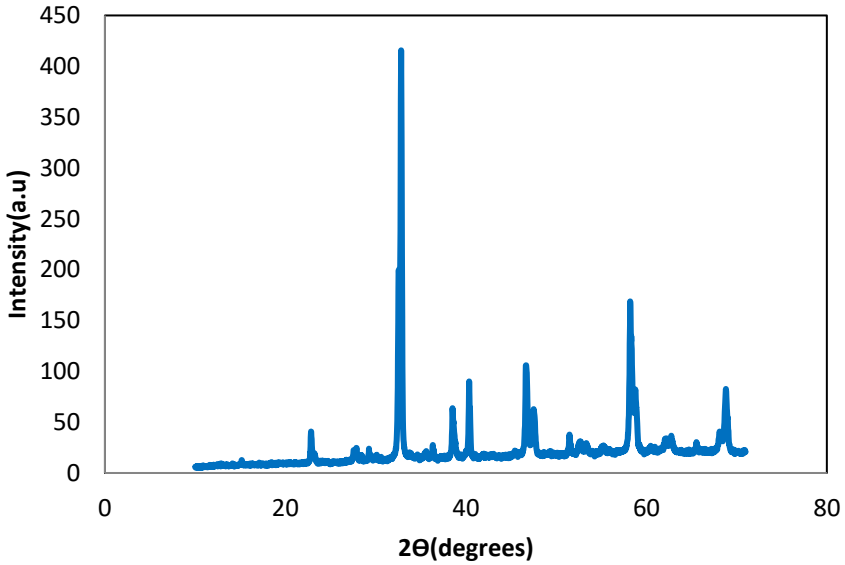

Figure6.2. .X-ray powder diffraction pattern of $YBa_2(Cu_{1-x}Zn_x)_3O_7.\delta$ (x=0.0)

Copyright *Author (s) 2026. Distributed under Creative Commons CC BY 4.0*
Received: *18-09-2026 -* ***Accepted:*** *16-11-2026 -* ***Published:*** *24-11-2026*

https://doi.org/10.54361/ajmas.261148

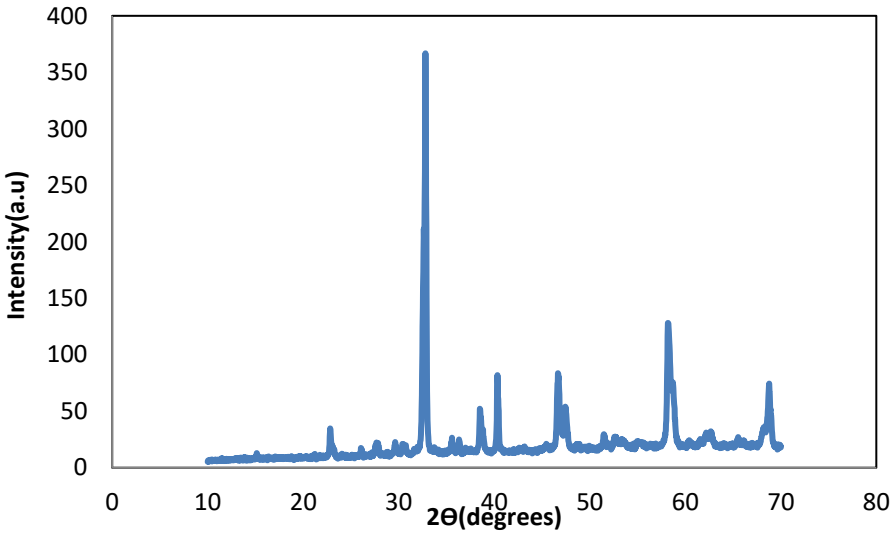

Figure6.3. .X-ray powder diffraction pattern of $YBa_2(Cu_{1-x}Zn_x)_3O_{7-\delta}$ (x=0.01)

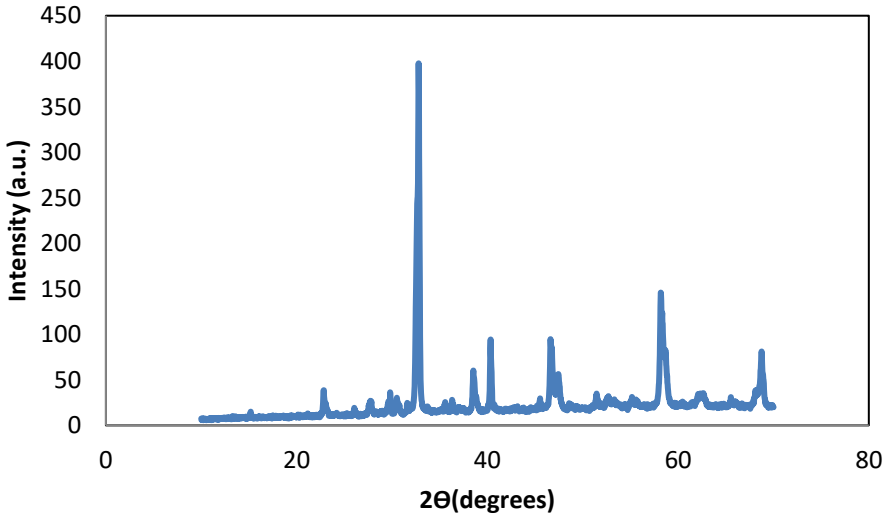

Figure6.4. .X-ray powder diffraction pattern of $YBa_2(Cu_{1-x}Zn_x)_3O_{7-\delta}$ (x=0.02)

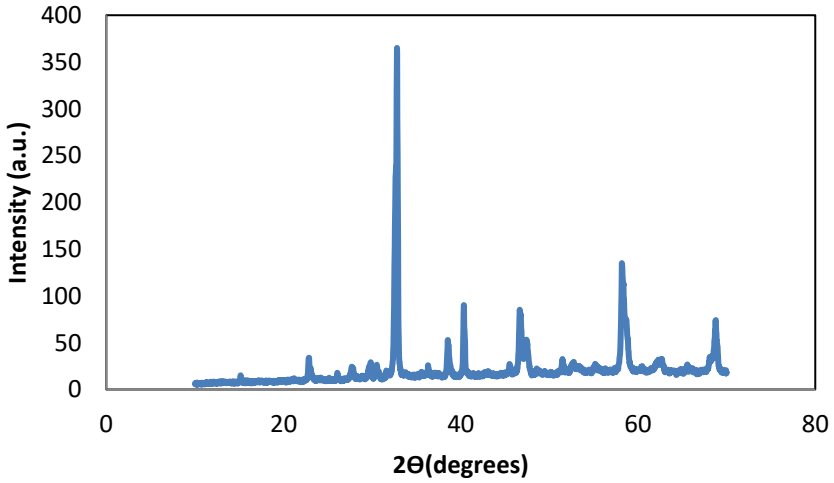

Figure6.5. .X-ray powder diffraction pattern of $YBa_2(Cu_{1-x}Zn_x)_3O_{7-\delta}$ (x=0.03)

Copyright *Author (s) 2026. Distributed under Creative Commons CC BY 4.0*
Received: *18-09-2026 -* ***Accepted:*** *16-11-2026 -* ***Published:*** *24-11-2026*

https://doi.org/10.54361/ajmas.261148

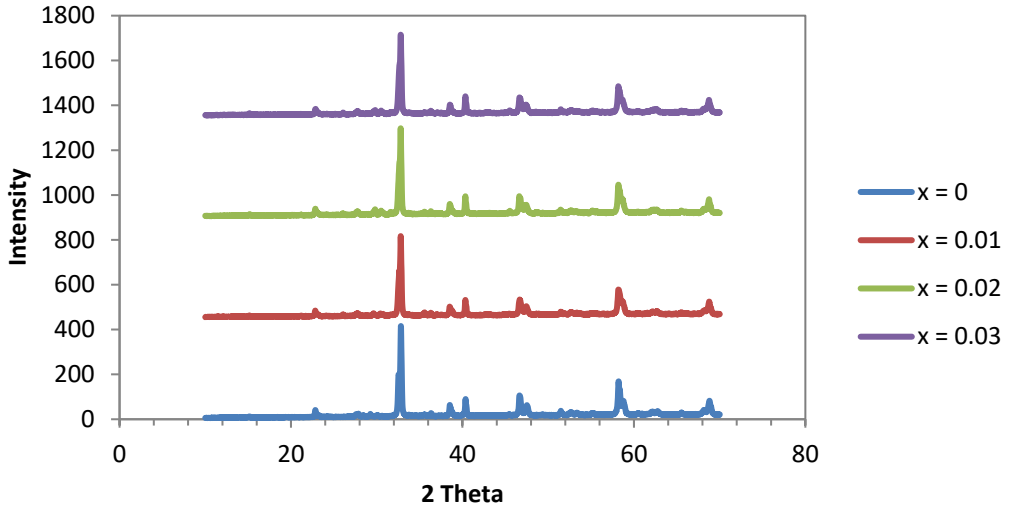

Figure6.6. .X-ray powder diffraction pattern of $YBa_2(Cu_{1-x}Zn_x)_3O_{7-}\delta$ for x=0, 0.01, 0.02, 0.03

X-ray diffraction results for the $YBa_2(Cu_{1-x}Zn_x)_3O_{7-}\delta$ (x = 0.00, 0.01, 0.02 and 0.03) samples are illustrated in Figures 6.2 to 6.5. The calculated lattice parameters a, b and c are shown in Table4. Figure 6.1 shows lattice parameters a, b and c/3 versus composition (x). Powder X-ray diffraction patterns (Fig.6.6) showed all samples to be single-phased with an orthorhombic structure $a \neq b \neq c$; some minor impurity peaks were observed. Fig.6.1 shows a slight increase in the a-lattice parameter and a decrease in the b-lattice parameter from (x=0) to (x=0.01), but after being doped with Zn, approximately constant a- and b-lattice parameters were observed between all the samples (x = 0.01, 0.02 and 0.03) with nearly constant volume. No systematic correlation between Zn content (x) and c-lattice parameter was observed.

Microstructure

The study of the microstructure of samples was carried out by scanning electron microscopy (SEM). SEM images of YBCO samples with compositions x = 0, 0.01, 0.02 and 0.03 are shown in (Figures 7.1 to 7.4).

Table5. Grain size of $YBa_2(Cu_{1-x}Zn_x)_3O_{7-}\delta$ with different compositions

Composition x	Grain size (μm)
0.00	1.5 μm
0.01	1.2 μm
0.02	1.2 μm
0.03	1.2 μm

SEM of the pure sample shows the formation of rectangular block grains aligned in some preferred directions. The grains of the pure sample (Figure7.1) have an average grain size of ~ 1.5 μm, and some gaps and voids were also observed. The results show a clear change in grain size between the pure sample and other samples doped with Zn. The grain size decreased from (x=0) to (x=0.01). But, in (Fig7.2,7.3 and 7.4) show that no significant variation in microstructure was observed between all the samples doped with Zn. On the other hand, the substitution of Zn does not have a considerable effect on microstructure in the $YBa_2Cu_3O_7$ system. The average grain size of all the samples with (x = 0.01, 0.02 and 0.03) of ~ 1.2 μm, and some gaps and voids were also observed.

Copyright *Author (s) 2026. Distributed under Creative Commons CC BY 4.0*
Received: *18-09-2026 -* ***Accepted:*** *16-11-2026 -* ***Published:*** *24-11-2026*

https://doi.org/10.54361/ajmas.261148

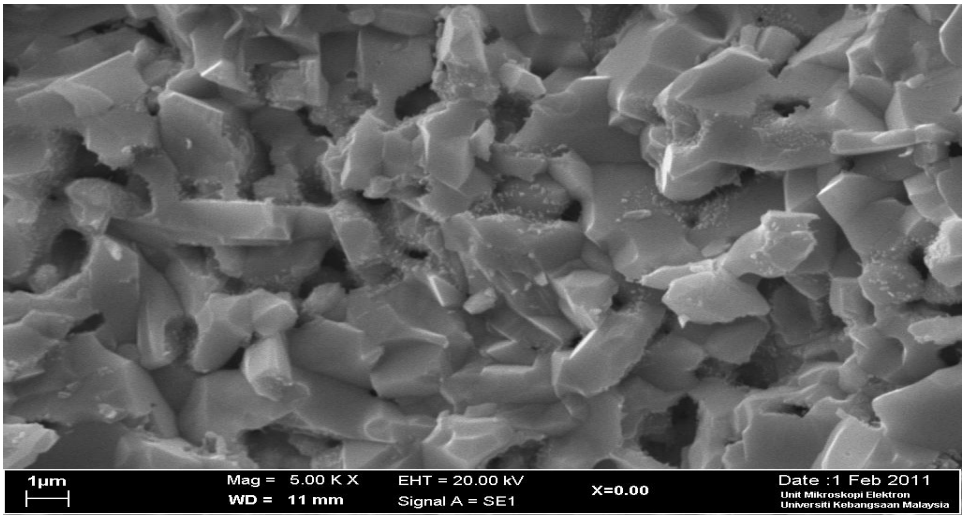

Figure7.1. SEM images of $YBa_2(Cu_{1-x}Zn_x)_3O_{7-}\delta$ with x = 0.00

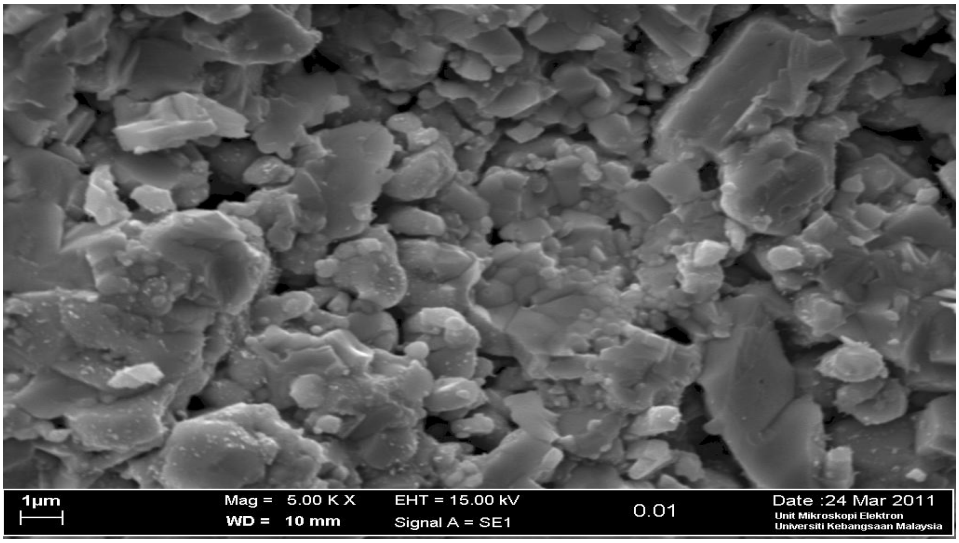

Figure7.2. SEM images of $YBa_2(Cu_{1-x}Zn_x)_3O_{7-}\delta$ with x = 0.01

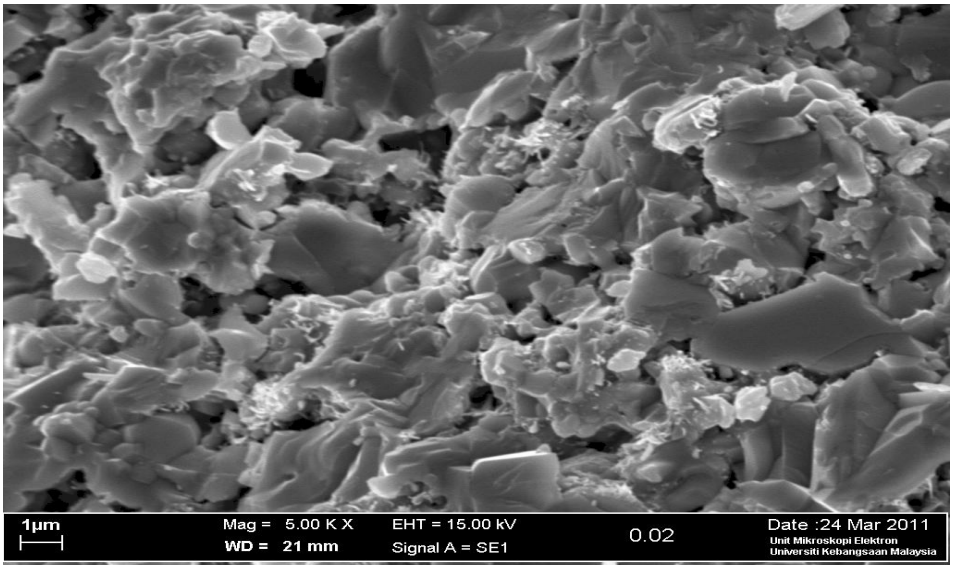

Figure7.3. SEM images of $YBa_2(Cu_{1-x}Zn_x)_3O_{7-}\delta$ with x = 0.02

Copyright *Author (s) 2026. Distributed under Creative Commons CC BY 4.0*
Received*: 18-09-2026 -* ***Accepted****: 16-11-2026 -* ***Published****: 24-11-2026*

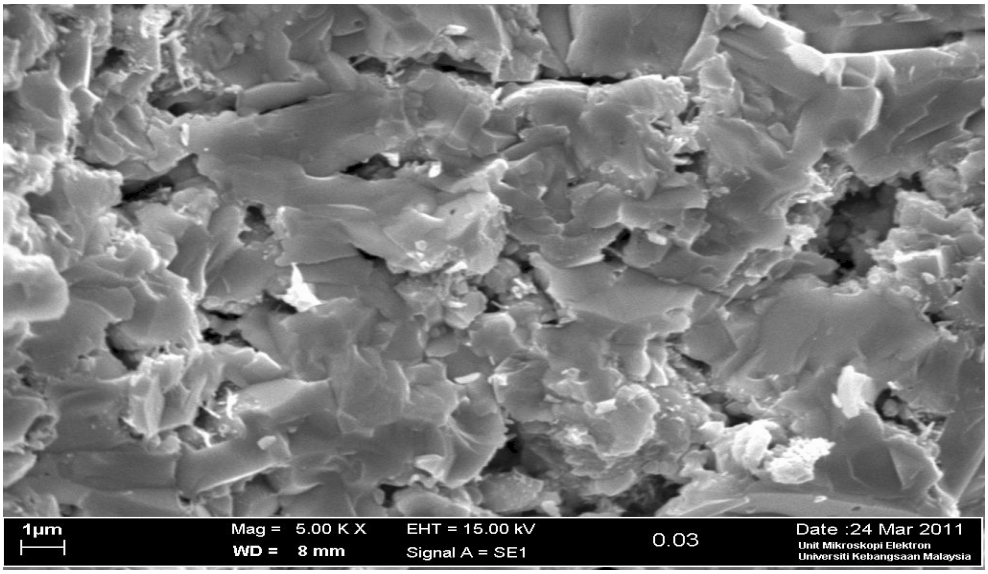

Figure7.4. SEM images of $YBa_2(Cu_{1-x}Zn_x)_3O_{7-}\delta$ with x = 0.03

Conclusion

In this study, the effect of Cu substitution by Zn on the superconducting properties of the $YBa_2(Cu_{1-x}\ Zn_{\ x})_3O_{7-}\ \delta$ superconductor with x = 0, 0.01, 0.02 and 0.03 was investigated by using the solid state reaction method. The pure sample, which exhibits T_c(zero) = 88 K and T_c (onset) around 95K, showed an average grain size of~ 1.5µm and some gaps and voids were also observed. In the measurement of dc resistance versus temperature, the transition temperature to superconductivity $T_c$was decreased with the increasing of Zn concentration. The width of phase transition ΔT_c exhibited a gradual decrease with more Zn doping. The decrease of T_c can be attributed to two possible mechanisms; in part it is due to the Zn ion acting as a strong in-plane scattering centre and, in part is due to the loss in oxygen content as Zn is substituted for Cu. The Zn cations substituted for Cu all go to occupy the Cu planar site. This substitution leads to a change in oxygen content and local lattice distortion. The Zn cations give rise to redistribution of charge that produces strong electron scattering, which breaks the coupling between Cooper pairs, therefore decreasing T_c rapidly. While the changed oxygen content decreases the itinerant hole density and hence T_c. The Van der Pauw method showed electrical resistivity of the samples at room temperature increases when Zn replaces Cu with increasing x. The sample x = 0.03 showed the highest electrical resistivity, $4\times 10^{-5}\Omega$m. This increase of the resistivity value with increasing x implies that the primary effect of Zn scattering is to add a nominally temperature-independent contribution to the transport scattering rate. Powder X-ray diffraction patterns showed all samples to be single-phased with an orthorhombic structure; some minor impurity peaks were observed. There is little variation in the lattice parameters that is due to the effect of different oxygen contents, and may be related to the effect of different ionic radii of Cu and Zn. SEM micrographs of $YBa_2(Cu_{1-x}Zn_x)_3\ O_{7-\delta}$ with Zn concentration (x) within the range of (0≤x≥ 0.03) showed that the grain size of the pure sample is ~ 1.5 µm, and some gaps and voids were also observed. The results show a clear change in grain size between the pure sample and other samples doped with Zn. The grain size decreased from x=0 to x=0.01. The change in the microstructure due to an increase in Zn concentration and is direct evidence of changes in the nature of the grain boundaries due to impurities. In addition, the shape of the grains showed a degree of irregularity and was distributed randomly with no alignment in a certain direction. And showed there is no significant variation in microstructure was observed between all the samples doped with Zn. Since it is well known that high scattering of electrons and consequently high resistivity values of the samples are due to more grain boundaries, more impurities and/or more crystal lattice defects (such as voids)

References

1. Abd-Shukor R. Introduction to Superconductivity in Metals, Alloys & Cuprates. Tanjong Malim: Penerbit Universiti Pendidikan Sultan Idris; 2004.
2. Holm W. Superconducting fluctuations as a tool to probe microscopic properties of YBa2(Cu1-xZnx)3O(7-δ). Stockholm: Department of Solid State Physics, Royal Institute of Technology; 1996. Report No.: S-100:44.
3. Krabbes G, Fuchs G, Canders WR, May H, Palka R. High Temperature Superconductor Bulk Materials. Berlin: Wiley-VCH; 2006.
4. Khare N. Introduction to High-Temperature Superconductors. New Delhi: National Physical Laboratory; 2003. Distributed by Marcel Dekker.
5. Wu MK, Ashburn JR, Torny CJ, Hor PH, Meng PL, Gao L, Huang ZJ, Wang YQ, Chu CW. Superconductivity at 93 K in a new mixed-phase Y-Ba-Cu-O compound system at ambient pressure. Phys Rev Lett. 1987;58:908.
6. Skakle JMS. Crystal chemical substitutions and doping of YBa2Cu3Ox and related superconductors. Mater Sci Eng R. 1998;R23:1-40.
7. Plakida N. High-Temperature Cuprate Superconductors. New York: Springer; 2010.
8. Hazen RM, Finger LW, Angel RJ, Prewitt CT, Ross NL, Mao HK, Hadidiac CG. Crystallographic description of phases in the Y-Ba-Cu-O superconductor. Phys Rev B. 1987;35:7238-7241.

Copyright *Author (s) 2026. Distributed under Creative Commons CC BY 4.0*
Received*: 18-09-2026 -* ***Accepted****: 16-11-2026 -* ***Published****: 24-11-2026*

9. Bouchoucha F, Ben Azzouz M, Annabi M, Zouaoui M, Ben Salem. The study on the ZnO and Zn0.95Mn0.05O added YBCO system: investigation of microstructure and transport properties. Physica C. 2010;470:262-268.
10. Singhal RK. How the substitution of Zn for Cu destroys superconductivity in YBCO system. J Alloys Compd. 2010;495:1-6.
11. Mohanta A, Behera D. Effect of Ga and Zn doping on coherent transition of YBCO superconductor. Indian J Pure Appl Phys. 2009;47:676-680.
12. Yunhui Xu. Rare earth ion size effect on the physical properties of the doped RBa2Cu3O7-δ superconductor systems. J GCPD. 1999.

Copyright *Author (s) 2026. Distributed under Creative Commons CC BY 4.0*
Received*: 18-09-2026 -* ***Accepted****: 16-11-2026 -* ***Published****: 24-11-2026*